Biomaterials 32 (2011) 6900–6911

Contents lists available at ScienceDirect

Biomaterials

journal homepage: www.elsevier.com/locate/biomaterials

Effects of TiO_2 nanotubes with different diameters on gene expression and osseointegration of implants in minipigs

Na Wang [a], Hongyi Li [b,**], Wulong Lü [c], Jinghui Li [a], Jinshu Wang [b], Zhenting Zhang [a,*], Yiran Liu [a]

[a] Department of Prosthodontics, School of Stomatology, Capital Medical University, Tian Tan Xi Li No. 4, Beijing 100050, China
[b] Photoelectrochemical Research Group, School of Materials Science and Engineering, Beijing University of Technology, Beijing 100124, China
[c] Hospital and School of Stomatology, Tianjin Medical University, Tianjin 300070, China

ARTICLE INFO

Article history:
Received 25 April 2011
Accepted 9 June 2011
Available online 5 July 2011

Keywords:
TiO_2 nanotubes
Gene expression
Osseointegration
In vivo
Implant
Minipig

ABSTRACT

Titanium dioxide (TiO_2) nanotubes can accelerate the adhesion and differentiation of osteoblasts, yet little is known how this nano-modified implant surface affects osseointegration at molecular level *in vivo*. The aim of this study was to investigate the effects of TiO_2 nanotubes with different diameters (30 nm, 70 nm and 100 nm) on biological attachment mechanism of implants to bone *in vivo* by studying the gene expression and bone formation around the implants. The histological features and fluorochrome labeling changes of bone around implants on the non-decalcified sections (at 3, 5 and 8 weeks after implantation) were investigated by using traditional light- and fluorescent microscopy, and the gene expression of alkaline phosphatase (*ALP*), osterix (*Osx*), collagen-I (*Col-I*) and tartrate-resistant acid phosphatase (*TRAP*) was examined by using real-time PCR at 1, 2, 3, 4 and 5 weeks after implantation. Comparing with machined titanium implants, a significant increase in bone–implant contact (BIC) and gene expression levels was found in the bone attached to implants with TiO_2 nanotubes, especially with 70 nm diameter nanotubes. At the same time, the sequential fluorescent labeling images illustrated dynamic bone deposition. In conclusion, TiO_2 nanotubes can modulate bone formation events at the bone–implant interface as to reach favorable molecular response and osseointegration; in addition, the diameters of nanotubes can be precisely controlled in order to obtain better bone formation.

1. Introduction

A rapidly established, strong and long lasting connection between an implant and bone is essential for the clinical success of orthopedics and dental implants. Implant topography is critical to the success of bone-anchored implant [1,2], so the technology of surface modification has been studied to promote osseointegration around the implant. Titanium (Ti) is an ideal metal for intra-osseous implants for its favorable biocompatibility and corrosion resistance. Many techniques have been developed to further enhance the bioactivity of pure Ti surface, such as sol–gel techniques, chemical treatment (alkali/acid/peroxidation treatment), anodization, magnetron sputtering, plasma spray, ion implantation, electrophoresis, lasers technique, self-assembly of monolayers [3–12], etc. The surface properties of Ti implants influence biological responses in the interface between bone tissue and implants and, consequently, their osseointegration [4,5,7,8]. In recent years, nanoscale surface modification has been attracting increasing attention. Several investigators had revealed that nanoscale topography influences cell adhesion and osteoblast differentiation. These findings reiterate observations demonstrating that nanotopography may directly influence adherent cell behavior [1,13–15].

After being treated with controlled anodizing method, a self-organized and highly ordered coating of Ti and Ti-based alloys–TiO_2 nanotubes was produced [6]. In previous studies, the titanium dioxide (TiO_2) nanotubes improved osteoblast adhesion, proliferation and exhibited strong bonding with bone [16–18]. It had been reported that cell fate was determined by the TiO_2 nanotube sizes *in vitro* [19–21], but optimum scale was controversial. To our knowledge, there is little animal experiment for studying the effect of different nanotube diameters on osseointegration of titanium implants. In addition, the underlying cellular and molecular mechanism responsible for the favorable osteogenesis responses to TiO_2 nanotubes is a complex biological process

* Corresponding author. Tel./fax: +86 10 67099279.
** Corresponding author. Tel./fax: +86 10 67391101.
E-mail addresses: lhy06@bjut.edu.cn (H. Li), yuhuashi69@163.com, wangming772003@yahoo.com.cn, zztttxl@hotmail.com (Z. Zhang).

0142-9612/$ – see front matter © 2011 Elsevier Ltd. All rights reserved.
doi:10.1016/j.biomaterials.2011.06.023

not fully understood yet, therefore, it is necessary to examine the interfacial cell functions and histological features. As a promising new tool to spatially and temporally analyze biological processes in cells or tissue with a high level of precision and accuracy, real-time polymerase chain reaction (real-time PCR) technique has been used in many *in vitro* studies analyzing the interactions between cells and biomaterial surfaces [13,14,16,22]. However, few *in vivo* studies by real-time PCR are available [23,24], and detailed *in vivo* studies on bone responses to TiO_2 nanotubes surface have not been reported.

Therefore, the purpose of our study was to investigate the effects *in vivo* of nanotube sizes on gene expression response and bone deposition surrounding implants, and we tried to explain the mechanisms and found out the optimum diameter of TiO_2 nanotube for early ossiointegration. At 3, 5 and 8 weeks after implantation, bone–implant contact (BIC) and fluorochrome labeling were analyzed using traditional light- and fluorescent microscopy. At 1, 2, 3, 4 and 5 weeks after implantation, gene expression of osteoblast (*osterix*, *ALP* and *collagen-I*) and osteoclast (*TRAP*) markers from implant surfaces and peri-implant bone tissue was detected using real-time PCR. The role of distance of cells to the implant was also assessed by comparing the gene expression of cells at the immediate vicinity of the implant surface to that detected in the peri-implant bone.

2. Materials and methods

2.1. Implants and treatments

Titanium cylinder implants (3.3 mm in diameter and 8 mm in height) were made by a company (LEIDEN, BeiJing, China) according to our order, and the implant surfaces were machined. A portion of pure titanium cylinder implants was treated by anodization [25]. The implants were rinsed in an ultrasonic bath of acetone, ethanol and distilled water respectively for 10 min. The cleaned pure titanium cylinder implants were anodized using graphite foil as counter cathode in glycerol electrolyte containing 0.3% NH_4HF_2 under magnetic stirring. The anodization voltage was 10 V, 20 V, 30 V respectively and the anodization time was 2 h. After being anodized, specimens were rinsed with distilled water several times, dried in air at 80 °C, and heat treatment performed at 500 °C for 2 h to crystallize the amorphous TiO_2 nanotubes into anatase structure.

The morphologyand alignment of the TiO_2 nanotubes array thin films were characterized by using field emission scanning electron microscopy (FESEM; S4800) with an accelerating voltage of 15 kV or 5 kV. The phase compositions of the TiO_2 nanotube thin films were determined by X-ray diffraction (XRD) using a diffractometer with Cu K_α radiation.

Both machined and TiO_2 nanotube specimens were sterilized in an autoclave for *in vivo* experiment.

2.2. Animals and surgery

2.2.1. Animals

The pig is an especially suitable animal to evaluate bone remodeling as its physiological and anatomical characteristics allow the results obtained in pig to be compared with those obtained in humans [26].

Forty healthy male minipigs, approximately 10 months old, weighing 30–40 kg, were obtained from the Institute of Animal Science of China Agricultural University. All the animals were housed in a temperature-controlled room with 12 h alternating light–dark cycle and were given water and food ad labium throughout the study. All animals were acclimatized for at least 2 weeks before the study began. The experimental protocol in this study was reviewed and approved by the Animal Care and Use Committees of Capital Medical University, China.

2.2.2. Surgical procedure

Animals were randomly divided into 8 groups (n = 5 in each group); 3 groups for histological observation, and the other 5 groups were used for gene examination.

In each minipig, four implants of each type (machined, 30 nm nanotubes, 70 nm nanotubes, 100 nm nanotubes) were inserted in the frontal skull and a total amount of 160 implants were inserted into frontal skull of 40 minipigs (Fig. 1). Before all experimental procedures, minipigs were anesthetized with an intramuscular injection of a combination of ketamine chloride (6 mg/kg) and xylazine (0.6 mg/kg) (Institute of Military and Veterinary Science, Changchun, China). Surgery was performed under sterile conditions. After shaving and cleaning (5 mg/ml chlorhexidine in 70% ethanol) the front skull was exposed through an incision followed by skin and mucoperiosteum reflection with blunt instrument. Using a series of implant drills (2.3-mm round bur, 2.5-mm pilot drill, 2.8–3.2-mm reamer drill, 3.3-mm profile drill), four identical holes for implantation were drilled with a low speed (800 rpm) under profuse cooling normal saline (0.9% NaCl) irrigation. Four implants with different surfaces (machined, 30 nm nanotubes, 70 nm nanotubes, 100 nm nanotubes) were inserted by press-fit. The periosteum and skin of the wound were sutured in two layers. After surgery, the animals were allowed to move freely and to receive antibiotics for 3 days to prevent postsurgical infection.

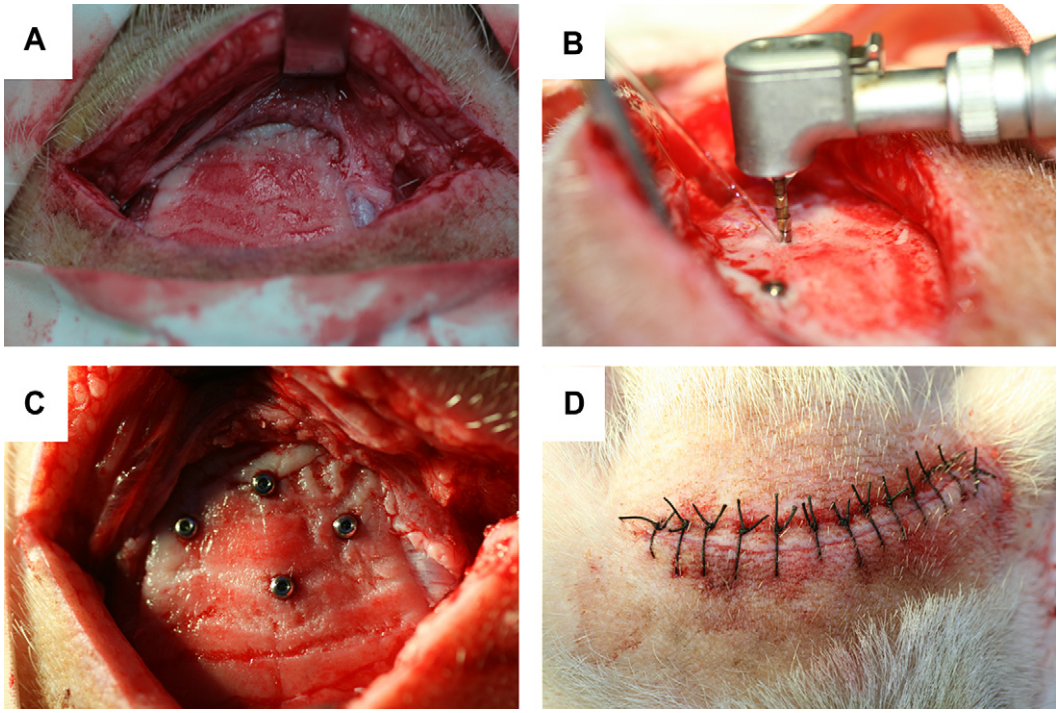

Fig. 1. Implantation surgery on minipig. (A) Incision and exposure of surgical fields. (B) Preparation of holes for implantation. (C) Placement overview of the 4 different implants. (D) Suture of wound.

Table 1
Polychromic fluorescence marking schedule for Group I, Group II and Group III.

Group (n = 5)	Xylenol orange (90 mg/kg)	Calcein (30 mg/kg)	Alizarin complexone (20 mg/kg)	Enthanasia
I	1 w	2 w		3 w
II	2 w	4 w		5 w
III	2 w	4 w	7 w	8 w

2.3. Bone labeling with fluorochromes

Polyfluorochrome tracers (xylenol orange, calcein and alizarin complexone) were injected intravenously as indicated in Table 1. Details had been published previously [27]. Briefly, under anesthesia the minipigs were injected with xylenol orange (90 mg/kg, Sigma), calcein (30 mg/kg, Sigma) and alizarin complexone (20 mg/kg, Sigma) through ear vein. The minipigs were euthanized for sampling at 1 week after final injection of fluorochrome (Table 1).

2.4. Retrieval procedure of gene sample

The retrieval procedure was performed according to RNA preserving protocol at 1, 2, 3, 4 and 5 weeks after implantation under anesthesia. After exposure of implants, cover screws were unscrewed by an octagonal screw driver and implant retrievers were screwed in implants, then the implants with adherent tissue were pulled out and placed immediately in freezing tubes. Peri-implant bone was separated from the skull using a trephine with internal Ø 4.1 mm and placed immediately in freezing tubes. All samples were stored in liquid nitrogen for real-time PCR analysis. At the end of procedure, the 5 groups of animals (n = 5) were euthanized by an intravascular injection of 20% pentobarbital solution into an ear vein until cardiac arrest occurred.

2.5. RNA isolation and quantification

The implants with adherent bone were placed in RNA*later* solution. Peri-implant bone samples were triturated in liquid nitrogen, homogenized in RNA*later* solution using Automated Tissue Homogenization. Homogenized tissue lysates were collected by centrifugation and pipetting. Total RNA from the implant surface and from the surrounding bone was isolated using the Trizol (SUNBIO, Beijing, China) according to the manufacturer's protocol. Total RNA was quantified using UV spectrophotometry.

2.6. Real-time PCR analysis

Design of primers for *OSX*, *ALP*, *Col-I*, *TRAP* and *GAPDH* was performed using the Primer premier 5 and oligo 6-based software. Primers were designed to yield short amplicons and to interact well with SYBR Green I fluorescent dye for detection of the PCR products in real-time (Table 2). Reverse transcription was carried out using iScript cDNA Synthesis Kit (TIANGEN, Beijing, China). All cDNAs were subjected to polymerase chain reaction (PCR) for GAPDH mRNA as a test of RNA integrity and cDNA synthesis. Subsequently, equal volumes of cDNA were used to program real-time PCR reactions specific for mRNAs encoding *OSX*, *ALP*, *Col-I* and *TRAP*.

Real-time PCR was performed in duplicates using BioEasy SYBR Green I Real-Time PCR Kit Manual (SUNBIO, Beijing, China) in Line-Gene Real-Time PCR Detection System (BIOER, Hangzhou, China), a total volume of 50 μl of PCR mixture, which included 25 μl of 2× SYBR Mix, 1 μl of PCR Forward Primer, 0.3 μl of PCR Reverse Primer, 1 μl of Taq DNA Polymerase, 20.71 μl of double-distilled H_2O, and 2 μl of template cDNA, were loaded in each well of the PCR array. PCR amplification was conducted with an initial 2 min step at 95 °C followed by 45 cycles of 95 °C for 20 s, 59 °C for 25 s, and 72 °C for 30 s. The fluorescence was read at the end of the 72 °C step. Melting curves were recorded after the run by stepwise temperature increase (0.5 °C/1 s) from 70 to 95 °C.

Table 2
Oligonucleotide sequences of sense (S) and antisense (A) primers used in the real-time PCR of target and housekeeping genes and amplicon size (base pairs) of the resulting PCR products.

Gene	Primer sequence	Amplicon size (bp)
Osterix	S: 5′CGATGAGCTGGTCACCGATT-3′ A: 5′CTTCGGATCTGCGGAACTTCT-3′	146
ALP	S: 5′AAGAGCATGTGCGGGAAAGT-3′ A: 5′ GGAATTCCCAGACAGCACAAA-3′	100
Collagen-I	S: 5′ CACCAGTCACCTGCGTACAGAA-3′ A: 5′ ACGTCATCGCACAACACATTG-3′	112
TRAP	S: 5′ TGAGAATGGCTTGGGCTTTG-3′ A: 5′ AGGCGAAGCCACCTAGTGAGT-3′	134
GAPDH	S: 5′ ATGGCCTTCCGTGTCCCTACT-3′ A: 5′ TAGCCCAGGATGCCCTTGA-3′	137

The fluorescent signal from SYBR Green was detected immediately after the extension step of each cycle, and the cycle at which the product was first detectable was recorded as the cycle threshold. The housekeeping gene *GAPDH* was used as the internal control gene to normalize the quantities of target genes. The normalized relative mRNA quantities were calculated by the $2^{-\Delta\Delta CT}$ method and reported as fold induction. The experimental time points were at 1, 2, 3, 4 and 5 weeks after operation.

2.7. Histological analysis

2.7.1. Histological preparation

Group I was euthanized at week 3, Group II at week 5, and Group III at week 8 respectively. The implants and their surrounding tissues were retrieved en bloc and immersed in 4% neutral buffered formaldehyde. The specimens were dehydrated in an ascending ethanol series (70, 80, 90, 100%) and acetone (100%), and embedded in MMA for infiltration and polymerization. The embedded specimens were cut into sections parallel to the central portion of the long axis of the implants (EXAKT-300 cutting equipment, German), and the cut surface was glued to a slide and sections were ground to a thickness of 30–35 μm (EXAKT-400 grinding equipment, German).

2.7.2. Fluorochromes microscopy imaging

Time course of bone formation was analyzed by polyfluorochromic markers using fluorescence microscopy (BX61, Olympus, Japan) equipped with a quadruple filter block (X-Cite® 120Q, EXFO, Canada). Fluorochrome-labeled bone that formed around the implants was analyzed at 3, 5 and 8 weeks after implantation, the xylenol orange-labeled lines, calcein-labeled lines, alizaline complexone-labeled lines were observed in newly formed bone around the implants.

2.7.3. Histological observation

The sections were stained with methylene blue–basic fuchsin and observed using a computer-connected microscope (BX61, Olympus, Japan). Photomicrographs of the slides were obtained and bone growth around the implants was evaluated. The relative amount of bone–implant contact (BIC) was analyzed using a PC-based image analysis system (Image-Pro R Analyzer 7.0 Japan), all measurements were made from bottom to top on both sides of the implants.

2.8. Statistics

In this study, the data were showed in the form of mean values ± SD. All data were analyzed using one-way ANOVA plus LSD (Least Significant Difference Procedure) test ($p < 0.05$) with SPSS 13 software (SPSS Inc., Chicago, IL, USA).

3. Results

3.1. TiO_2 nanotubes and crystal structure of implant characterization

After anodization in the respective voltage (10 V, 20 V, 30 V) and annealing at 500 °C, the morphology of TiO_2 nanotube array thin films was characterized by using FESEM to ascertain the nanotubes dimensions (Fig. 2(a–c)). The nanotubes were found to have 30 nm (10 V), 70 nm (20 V) and 100 nm (30 V) outer diameter.

XRD diffraction patterns of nanotube films before and after being annealed at 500 °C are shown in Fig. 3. It is clear that, the as-anodized nanotube thin films were amorphous, and transferred into anatase after heat treatment at 500 °C for 2 h, the height of the peak of TiO_2 is comparatively low, which implies that the thickness of the nanotube array film is relatively small.

3.2. Gene expression

3.2.1. Gene expression of osteogenesis-related genes (OSX, ALP and Col-I) at implant surface

In comparison with machined implant surface, the expression of *OSX*, *Col-I* and *ALP* at 30 nm, 70 nm, 100 nm TiO_2 nanotubes implant surfaces was significantly higher, with the 70 nm TiO_2 nanotubes having the highest level of gene expression at all time points (Fig. 4(a–e), $p < 0.05$). The *OSX* expression was upregulated at week 1 and subsequently dropped to a low level at week 3, after that a second expression peak at week 4 occurred (Fig. 5(a)). For *ALP*, a high level of expression was observed at week 1, and subsequently decreased till week 3, after that the *ALP* expression increased continuously toward the end of the experiment

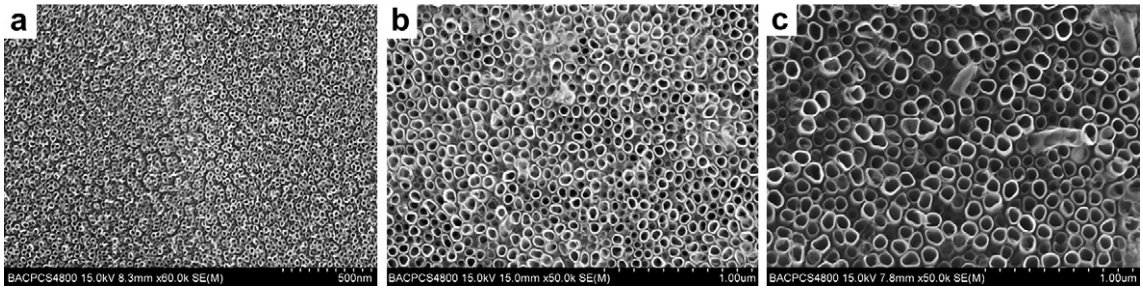

Fig. 2. TiO_2 nanotube (a–c) SEM micrographs (top view) of self-aligned TiO_2 nanotubes with different nanotube pore diameters created by controlling anodizing potentials. (a) 30 nm (10 V), (b) 70 nm (20 V), (c) 100 nm (30 V).

(Fig. 5(b)). For *Col-I*, the first peak of expression was at week 2, the second peak was at week 4, followed by a down-regulation after week 4 toward the end of experiment (Fig. 5(c)).

3.2.2. Gene expression in the bone around implants

A significant difference was demonstrated in the expression of *ALP* and *TRAP* between bone samples around machined implants and those around TiO_2 nanotubes implants at all specific time points (Fig. 6(a–e), $p < 0.00$). The highest level of gene expression was in the bone around implants with 70 nm TiO_2 nanotubes at 1, 2 and 3 weeks. The difference between 70 nm and 100 nm nanotubes was not significant at 4 and 5 weeks. However at all time points, the gene expression in the bone around 70 nm nanotubes implants was significantly higher than those around 30 nm nanotubes implants. Furthermore, the temporal pattern of the gene markers in bone around implants was similar to that seen at the implants surfaces. This pattern was characterized by a peak of *ALP* expression at 1 week and subsequent decrease till week 3, after that the *ALP* expression increased continuously toward the end of the experiment (Fig. 7(a)). For *TRAP*, the temporal pattern was upregulated to the first peak of expression at week 2, followed by a decrease at week 3, and the second peak was at week 4 with subsequent down-regulation toward the end of the experiment (Fig. 7(b)).

3.3. Histology

3.3.1. Clinical observations

All animals survived and recovered quickly from implant surgery, they appeared to be in good health throughout the test periods. Neither clinical signs of inflammation nor adverse tissue reactions were observed around the implants in the frontal skull.

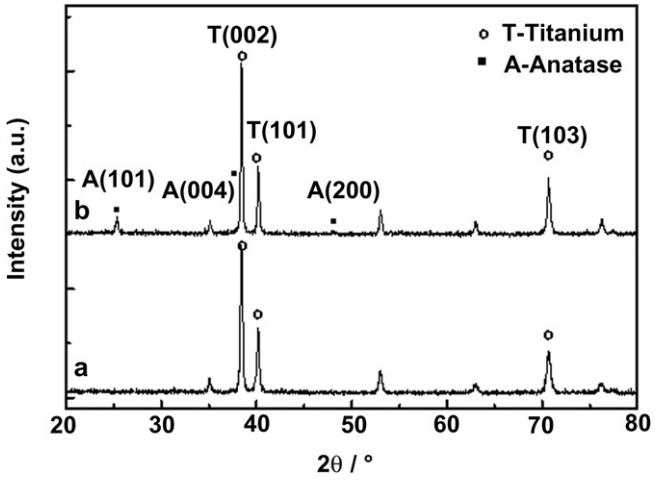

Fig. 3. XRD patterns of TiO_2 nanotube arrays before (a) and after heat treatment at 500 °C (b).

3.3.2. Histological observation and histomorphometry of bone–implant interface

At 3, 5 and 8 weeks after implantation, all implants in the control and test groups were histologically in direct contact with the surrounding bone, with no signs of inflammation at the bone–implant interface (Figs. 8–10). At 3 weeks after implantation, the original bone coloboma prepared by the drill could be recognized in each section filled with immature woven bone (Fig. 8). The newly formed bone trabeculae were characterized by osteoid arches including large and rounded osteoblasts and osteocytes. Some of newly formed bone extended from the surface of the parent bone into implant, and some was in direct contact with the implant surface (without an intervening fibrous tissue layers). Except for mineralized bone, the rest of implant surface was surrounded by non-mineralized osteoid matrix that was lined with osteoblasts. Rod-like trabeculae gradually became mature during 5–8 weeks after implantation. At 5 weeks after implantation, the woven bone was reinforced by the deposition of parallel-fibered bone, and bone density evidently increased. The trabeculae of woven bone were lined by osteoblasts, indicating that bone formation was in progress (Fig. 9). At 8 weeks after implantation, lamellar structure could be seen in trabeculae bone, spaces of bone marrow in the woven bone became larger than those at 5 weeks. The bone marrow became more mature, which was filled with many adipose cells and fewer osteoblasts and vascular structures. Some narrow non-mineralized matrix was observed between the blue osteoblasts and the red mineralized bone, which indicated that osteogenesis was still in progress (Fig. 10).

At 3 weeks, direct bone–implant contact (BIC) with machined implants was $17.61 \pm 4.68\%$. At implants with 30 nm, 70 nm and 100 nm TiO_2 nanotubes surfaces, bone was more continuous along the implants surfaces, and direct bone–implant contact (BIC) was $36.18 \pm 5.32\%$, $55.46 \pm 9.71\%$ and $45.19 \pm 4.36\%$ respectively. The amount of BIC with the machined and 30 nm, 70 nm, 100 nm nanotubes implants was $29.14 \pm 6.61\%$, $52.80 \pm 7.96\%$, $71.04 \pm 5.3249\%$ and $62.14 \pm 6.18\%$ respectively, at 5 weeks after implantation. The amount of BIC with the machined and 30 nm, 70 nm, 100 nm nanotubes implants was $28.98 \pm 1.79\%$, $58.50 \pm 5.12\%$, $67.97 \pm 4.61\%$ and $67.12 \pm 6.36\%$ respectively, at 8 weeks after implantation. Thus, at weeks 3, 5 and 8, significantly more direct bone–implant contact (BIC) with TiO_2 nanotubes implants, especially the implants with 70 nm TiO_2 nanotubes (Fig. 11, $p < 0.05$) was found.

3.3.3. Fluorescence microscopy

Bone deposition with fluorescent labels was most noticeable in photomicrographic images shown in Figs. 12–14. At 3 and 5 weeks after implantation, the double fluorescent labels (green lines and

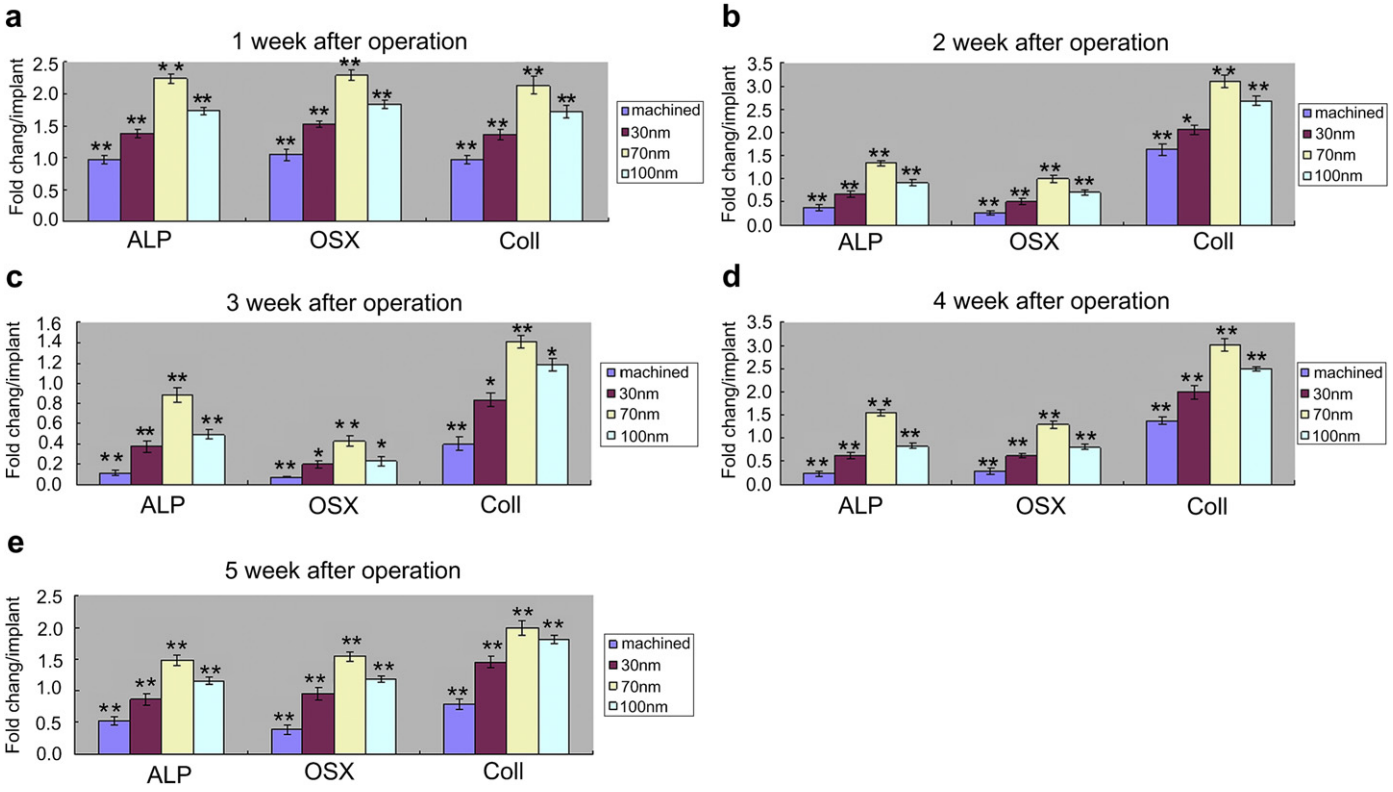

Fig. 4. The mRNA expression of the osteogenesis-related genes at implant surface. At 1, 2, 3, 4 and 5 weeks, the total RNA was isolated and extracted from cells adhering to implants with machined, 30 nm nanotubes, 70 nm nanotubes and 100 nm nanotubes surfaces. The expression levels for *OSX*, *ALP*, *Col-I*, *TRAP* were compared for all surfaces. The results are shown in fold change ($2^{-\Delta\Delta CT}$ method, baseline = week 1 expression at machined implant surface). (a) 1 week, (b) 2 weeks, (c) 3 weeks, (d) 4 weeks, (e) 5 weeks. Asterisk (*) shows a significant difference in comparison with machined implant ($p < 0.05$), Double asterisks (**) show a significant difference in comparison with all other groups in the experiment ($p < 0.05$).

orange lines) in the bone around implants of control and test groups were very marked, calcein-labeled lines adjoining the marrow cavity were observed. At 3 weeks after implantation (in Group I), both xylenol orange-labeled (orange) and calcein-labeled lines (green) were very marked (Fig. 12). At 5 weeks after implantation (in Group II), the brightness of xylenol orange-labeled lines was diminished, calcein-labeled lines were more obvious than orange-labeled lines (Fig. 13). At 8 weeks after implantation (in Group III), alizarin-labeled lines (red) were most obvious, calcein-labeled lines (green) came second, xylenol orange-labeled lines (orange) were nearly invisible (Fig. 14). The fluorescent labels in the surrounding bone of TiO_2 nanotubes implants were more obvious

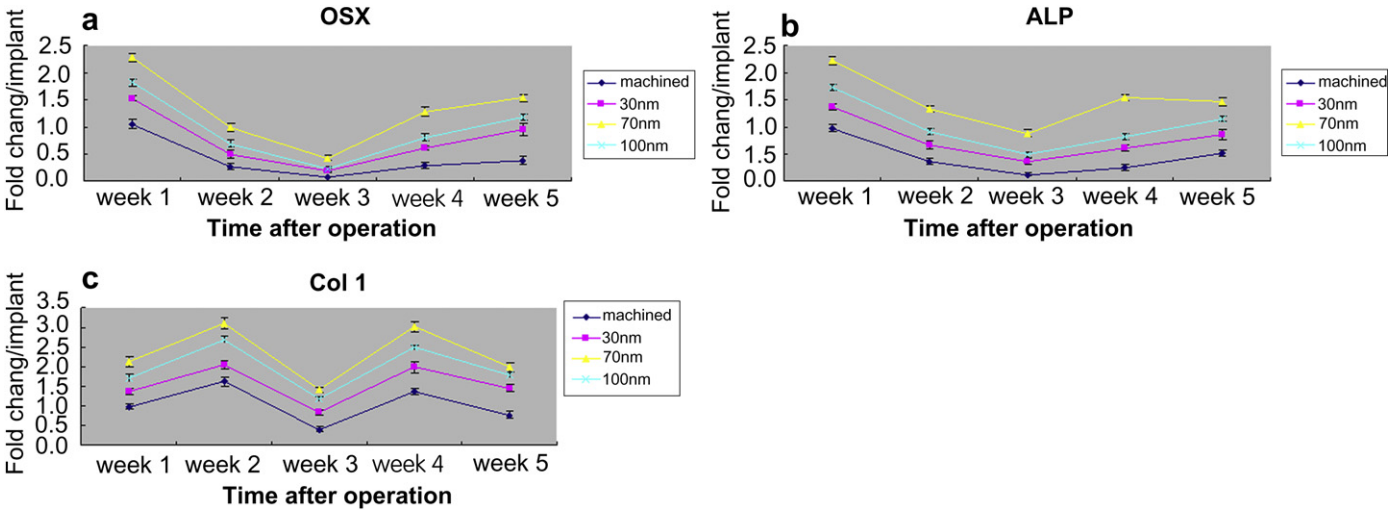

Fig. 5. Osteogenesis-related mRNA expression trend. Total RNA was isolated from cells at 1,2,3,4 and 5 weeks adhering to implants with machined, 30 nm nanotubes, 70 nm nanotubes and 100 nm nanotubes. The temporal pattern of expression levels for (a) *OSX*, (b) *ALP*, (c) *Col-I* is shown as fold change ($2^{-\Delta\Delta CT}$ method, baseline = week 1 expression at machined implant surface).

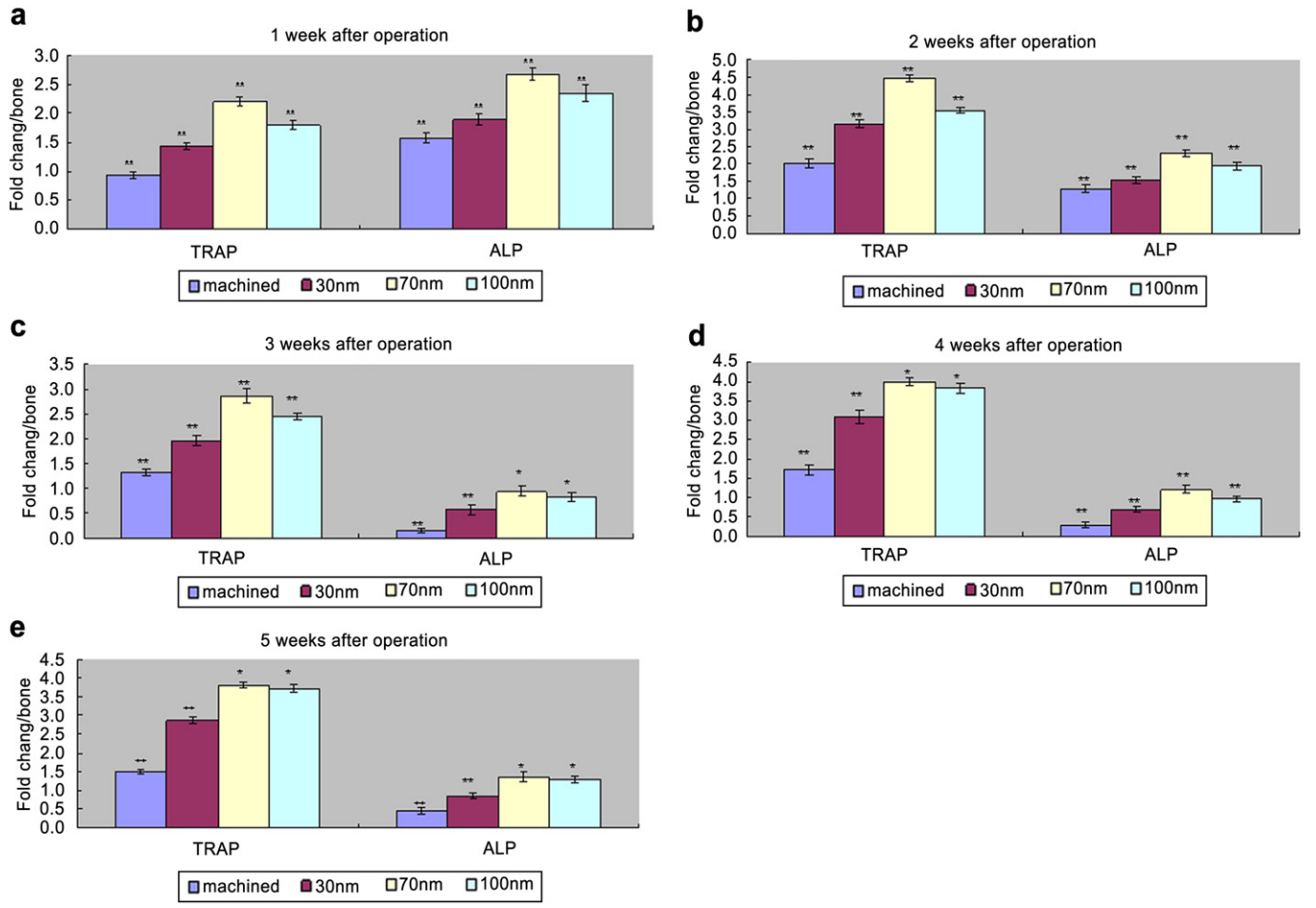

Fig. 6. *In vivo* gene expression trend of *ALP* and *TRAP* in bone around implants at 1, 2, 3, 4 and 5 weeks; total mRNA was isolated from bone around implants of machined, 30 nm nanotubes, 70 nm nanotubes and 100 nm nanotubes and analyzed by real-time PCR. Expression levels (fold change) for *ALP* and *TRAP* were compared for all surfaces. The results are shown in fold change ($2^{-\Delta\Delta CT}$ method, baseline = week 1 gene expression in bone surrounding machined implants). (a) 1 week, (b) 2 weeks, (c) 3 weeks, (d) 4 weeks, (e) 5 weeks. Asterisk (*) shows a significant difference in comparison with machined implant ($p < 0.05$). Double asterisks (**) show a significant difference in comparison with all other groups in experiment ($p < 0.05$).

and continuous than those of machined implants, especially those around 70 nm TiO_2 nanotubes implants.

4. Discussion

The results of our study demonstrate that TiO_2 nanotube layer significantly enhanced osteogenesis gene expression, bone–implant contact and bone deposition of pure titanium implants, and of all different TiO_2 nanotubes implants, the optimum size of nanotube for osseointegration was 70 nm diameter.

In our study, the high osteogenesis-related expression and rapid bone formation on TiO_2 nanotubes could attribute to its special nanostructure. Nanostructure surfaces possess unique properties that influence molecular and cellular activities and alter the process of osseointegration by direct and indirect mechanisms [1,13–15]. Several previous studies had demonstrated the beneficial effects of TiO_2 nanotubes on osteoblast differentiation and bone formation around implants *in vivo* and *in vitro* [16–18,21]. Vertically aligned TiO_2 nanotubes exhibit enormously larger surface areas than the flat Ti surface, and

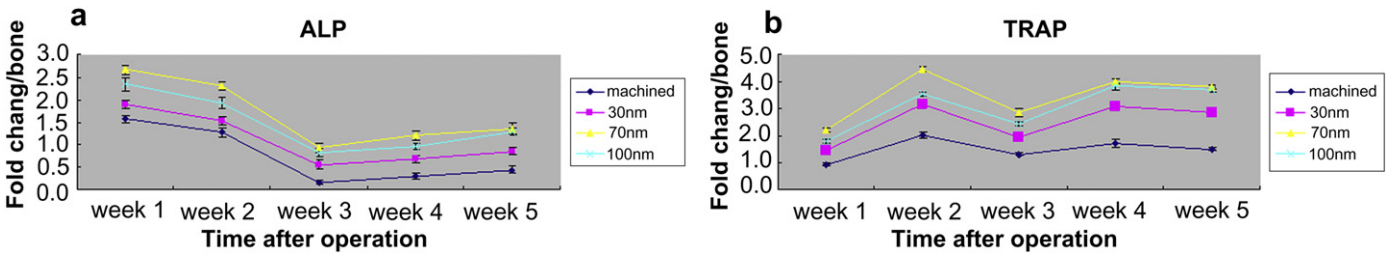

Fig. 7. *In vivo* gene expression trend of *ALP* and *TRAP* in bone around implants. Total RNA was isolated at 1, 2, 3, 4 and 5 weeks from bone around implants of machined, 30 nm, 70 nm and 100 nm nanotubes. The temporal pattern of expression levels for (a) *ALP*, (b) *TRAP* is shown as fold change ($2^{-\Delta\Delta CT}$ method, baseline = week 1 expression at machined implant surface).

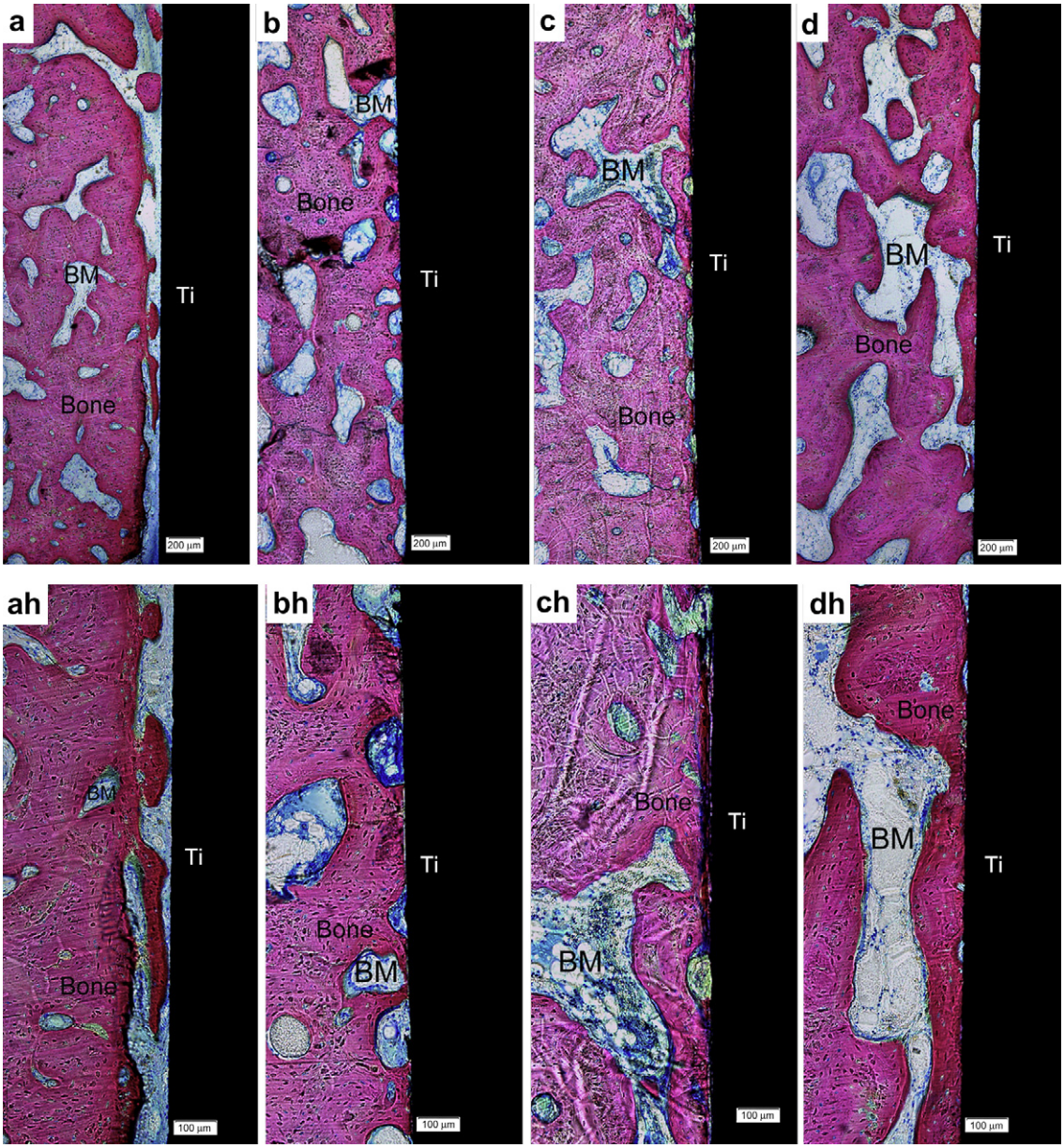

Fig. 8. Digital photographs of stained (methylene blue/basic fuchsine) histological sections at 3 weeks after implantation. Implant in the image is (a) machined, (b) 30 nm TiO_2 nanotubes, (c) 70 nm TiO_2 nanotubes, (d) 100 nm TiO_2 nanotubes. The high magnification of interface between bone and implant is shown in (ah) to (dh) which correspond to machined, 30 nm, 70 nm, 100 nm, respectively. Bone is pink/red, osteoblasts are blue and Ti alloy is black, Ti = titanium, BM = bone marrow. (For interpretation of the references to color in this figure legend, the reader is referred to the web version of this article.)

contribute to the interlocked cell configuration. TiO_2 nanotube structure is discrete with a gap between adjacent nanotubes (see Fig. 2). Such a sub-division structure is important for minimizing the interfacial stresses between two dissimilar materials joined together and can allow the passage of body fluid which supplies the nutrient for cell growth. Meanwhile, the TiO_2 nanotubes surface can mimic the dimensions of components of natural bone, because natural bone is composed of nanophase hydroxyapatite in the collagen matrix [28]. It is well established that the anatase phase TiO_2 is much more efficient in nucleation and growth of Hap than the rutile phase TiO_2 presumably because of the better lattice match with Hap phase [29], so all specimens in this study were annealed at 500 °C after anodization to get anatase TiO_2 nanotubes surface.

The skull of pig is flat bones with two parallel layers of compact bone sandwiching a layer of spongy bone. Intramembranous ossification mainly occurs during process of skull formation. After implantation, the formation of mineralized bone near implant surface requires the colonization of implant surface by osteoblastic cells, these cells mainly originate from mesenchymal stem cells (MSCs) recruited by implant surface [30,31]. MSCs differentiate into osteogenitor cells, and then into osteoblasts. Osteoblasts synthesize osteoid that is mineralized to form new bone.

Bone formation is an intricate and ordered cascade of synthesis of matrix proteins and calcium phosphate in a continuously renewed biological environment and regulated by a cluster of growth factors. In bone formation, osteogenesis-related genes are strictly regulated to ensure correct chronological order and each gene has a unique expression profile [13,14,16,22,24,31–33]. In our study, gene expression also showed unique characteristics. *Osterix* (*Osx*) is a zinc finger transcription factor specifically expressed by osteoblasts which is important for osteoblast differentiation. *Osx*

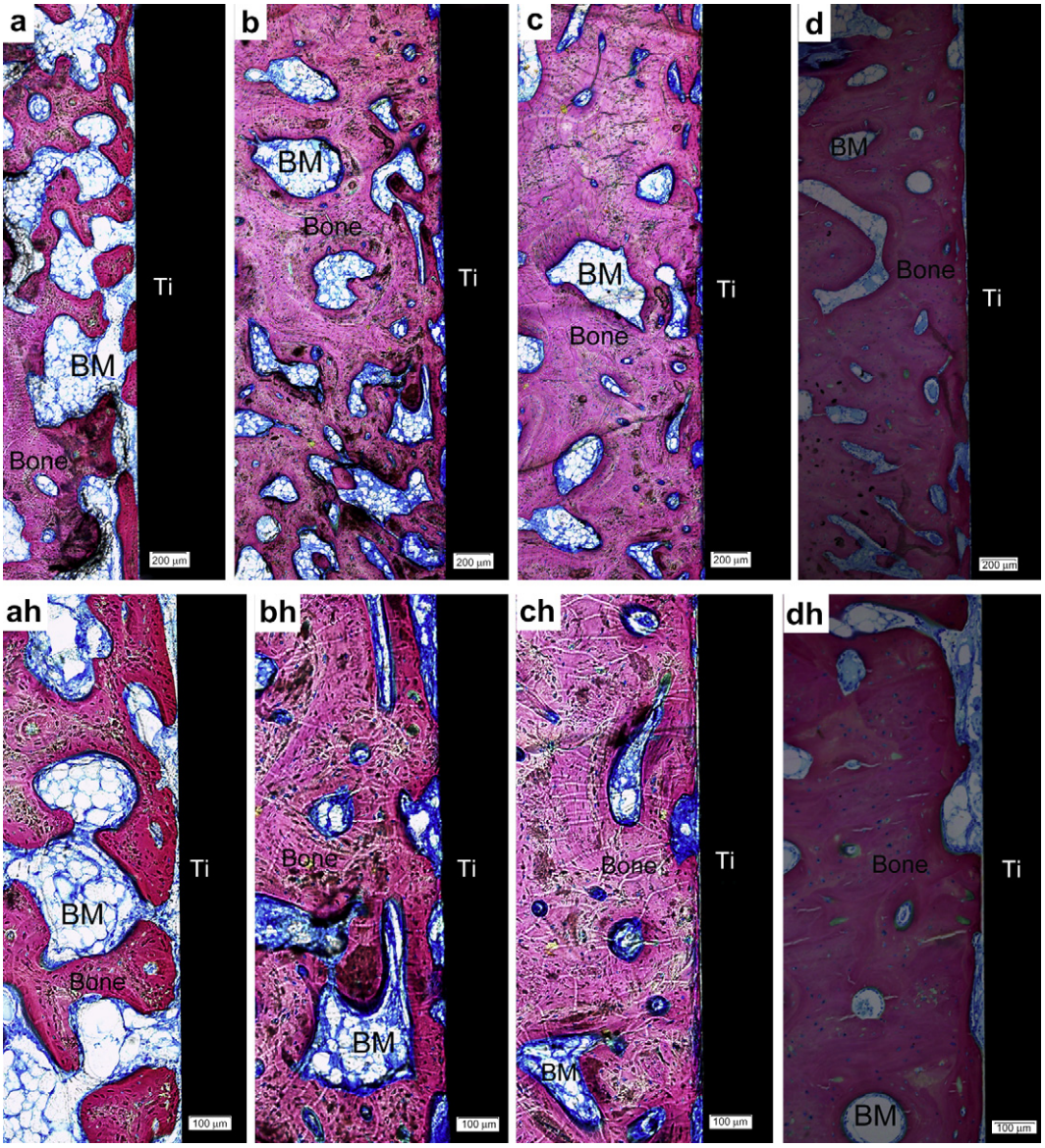

Fig. 9. Digital photographs of stained (methylene blue/basic fuchsine) histological sections at 5 weeks after implantation. Implant in the image is (a) machined, (b) 30 nm TiO_2 nanotubes, (c) 70 nm TiO_2 nanotubes, (d) 100 nm TiO_2 nanotubes. The high magnification of interface between bone and implant is shown in (ah) to (dh) which correspond to machined, 30 nm, 70 nm, 100 nm, respectively. Bone is pink/red, osteoblasts are blue and Ti alloy is black, Ti = titanium, BM = bone marrow. (For interpretation of the references to color in this figure legend, the reader is referred to the web version of this article.)

transcription acts by directing pre-osteoblasts to immature osteoblasts. *Osx*-deficient mice show absence of osteoblasts and defective bone formation [34]. In our study, the expression of *Osx* peaked at an earlier time points (week 1), suggesting its importance for osteoblast differentiation, as has been reported in other studies of osteoblast differentiation [32–35]. The expression of *Osx* was significantly higher at 70 nm nanotubes surface than at other surfaces in our study, which demonstrated that 70 nm was optimum size for TiO_2 nanotubes to induce osteoblast differentiation. As an osteoblast-specific gene, *ALP* is active in osteoblast differentiation and new matrix formation. In cell differentiation, the increase of *ALP* activity commits more cells to differentiate into the osteoblast lineage [13,14,31,32]. Mineralization involves osteoblasts secreting vesicles containing alkaline phosphatase, the vesicles rupture and act as a center for crystals to grow on, then mineral crystals distributed among the collagen fibrils. Type I collagen is the most important fibrillar type of collagen extracellular matrix component and serves as mineralization scaffolds and hydroxyapatite initiation sites [36]. *Col-I* is known to be an early osteogenitor marker and necessary to bone matrix formation [32,33]. In our study, *ALP* expression was upregulated at earlier time points (week 1), *Col-I* expression reached to the first peak at later time points (week 2). At all time points, 70 nm TiO_2 nanotubes surface had the highest expression level of *ALP* and *Col-I* comparing with other implant surfaces, suggesting that 70 nm was an optimum size for osteoblast differentiation, matrix formation and mineralization. The tartrate-resistant acid phosphatase (*TRAP*) is expressed at high levels in osteoclasts and is therefore used as a molecular marker for osteoclasts [37]. In our study, comparing with machined implants, the *TRAP* expression in bone around TiO_2 nanotubes implants, especially around 70 nm nanotubes implants, was higher, which was similar to osteoblast marker. This result suggests that *TRAP* expression is important in normal bone formation in spite of its resorption function, the high expression

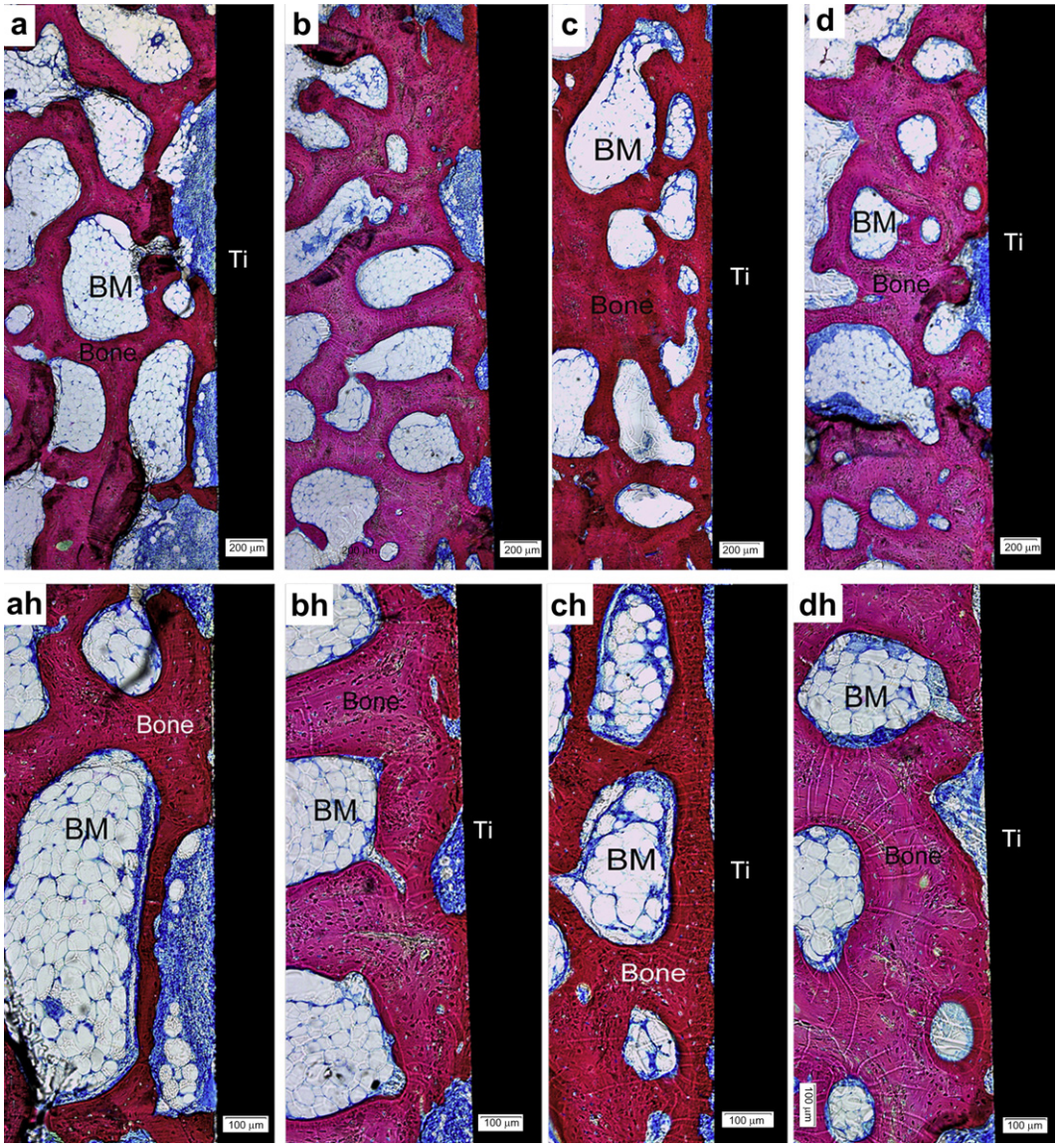

Fig. 10. Digital photographs of stained (methylene blue/basic fuchsine) histological sections at 8 weeks after implantation. Implant in the image is (a) machined, (b) 30 nm TiO_2 nanotubes, (c) 70 nm TiO_2 nanotubes, (d) 100 nm TiO_2 nanotubes. The high magnification of interface between bone and implant is shown in (ah) to (dh) which correspond to machined, 30 nm, 70 nm, 100 nm, respectively. Bone is pink/red, osteoblasts are blue and Ti alloy is black, Ti = titanium, BM = bone marrow. (For interpretation of the references to color in this figure legend, the reader is referred to the web version of this article.)

of bone formation and bone resorption marker indicate an active formation and remodeling throughout the time periods concomitant with an increasing ossiointegration of TiO_2 nanotubes implants to bone. The result is in agreement with previously published data where normal *TRAP* expression was indispensable to bone formation and remodeling [38,39].

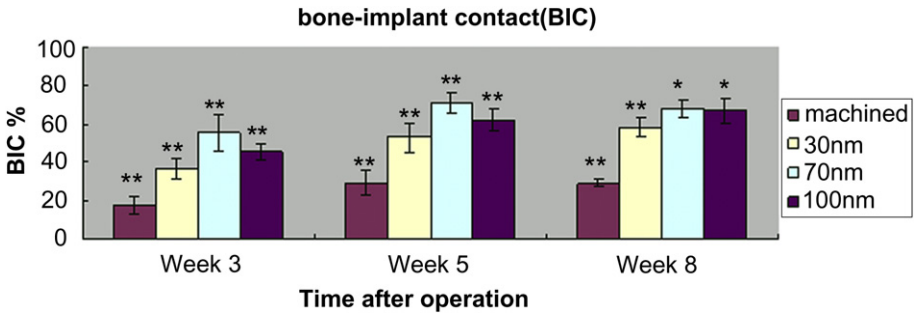

Fig. 11. The mean values with SD (error bars) of bone-implant contact (BIC) over the total implant length for all implant surfaces at 3, 5 and 8 weeks after implantation. Asterisk (*) shows a significant difference in comparison with machined implant ($p < 0.05$). Double asterisks (**) show a significant difference in comparison with all other groups in experiment ($p < 0.05$).

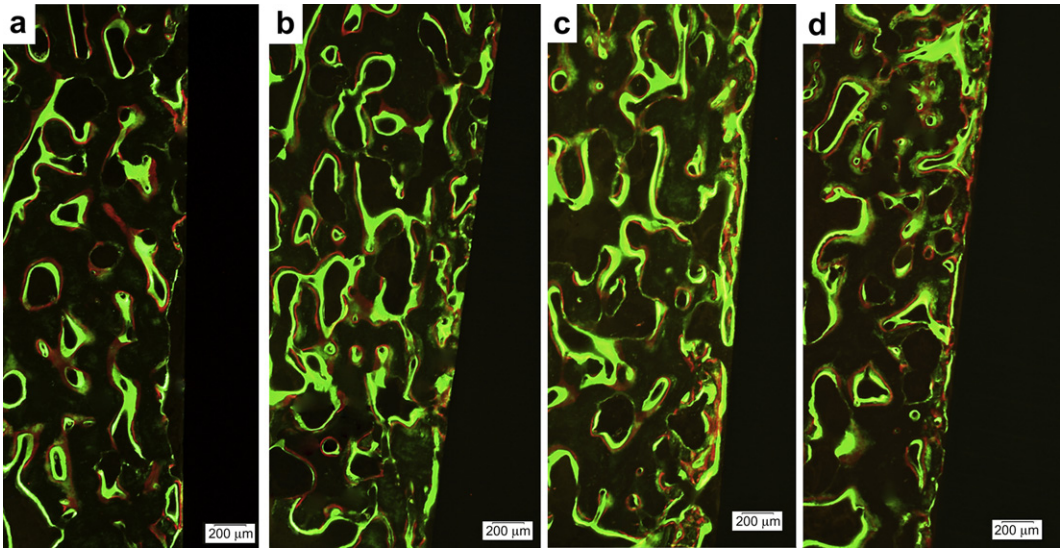

Fig. 12. Fluorescence microphotograph at 3 weeks after implantation. Fluorochrome analysis revealed new bone formation around all implants by the following markers: xylene orange-labeled lines (orange), calcein-labeled lines (green). Both labeled lines were very marked. (a) machined implant, (b) 30 nm TiO_2 nanotubes implants, (c) 70 nm TiO_2 nanotubes implants, (d) 100 nm TiO_2 nanotubes implants. (For interpretation of the references to color in this figure legend, the reader is referred to the web version of this article.)

In our study, the osteogenesis-related gene expression on TiO_2 nanotubes of 30 nm diameter is significantly lower than those on the nanotubes of larger diameter (70 nm and 100 nm), this phenomenon can be analyzed by molecular biomechanics. On TiO_2 nanotubes, protein aggregates adhere to the top wall surface owing to the presence of empty nanotube pore spaces and the gap between adjacent nanotubes [21]. MSCs are forced to elongate and stretch to search for protein aggregates to establish initial contact, this elongated morphology probably causes cellular cytoskeletal tension and stress, larger the nanotube size is, more the cellular cytoskeletal tension and stress on nanotubes are. It is well known that various kinds of physical stresses from the substrate morphology and topography can accelerate stem cell differentiation into a specific cell lineage [14,19,21,40,41], and our study has obtained similar data. However, gene expressions on 100 nm nanotubes were significantly lower than that on 70 nm nanotubes. Probably owing to the larger empty nanotube pore spaces, proteins on 100 nm TiO_2 nanotubes were more sparsely at the top wall surface than that on 70 nm nanotubes, so cells adhered to 100 nm nanotubes were less than cells on 70 nm nanotubes. With regard to the above-mentioned phenomenon, another probable important cause is that 70 nm is similar to the nanostructure of natural bone, and previously many groups had already verified the effect of mimicking the bone surface nanoroughness using various biomaterials [13–15]. In natural bone, collagen type-I forms fibrils with an interfibrillar spacing of 68 nm and 35 nm depth [36,42]. The hydroxyapatite crystals are embedded in fibrils and have an average size of $50 \times 25 \times 4\ nm^3$ [28]. With the effect of mimicking

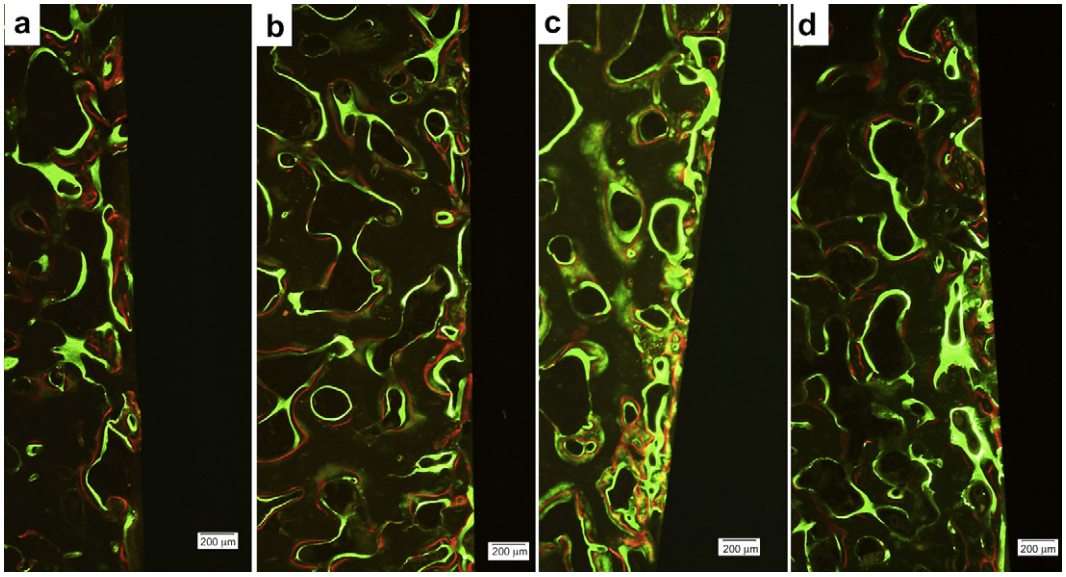

Fig. 13. Fluorescence microphotograph at 5 weeks. Fluorochrome analysis revealed new bone formation around all implants by the following markers: xylene orange-labeled lines (orange), calcein-labeled lines (green). The brightness of calcein-labeled lines were more obvious than xylenol orange. (a) machined impant, (b) 30 nm TiO_2 nanotubes implants, (c) 70 nm TiO_2 nanotubes implants, (d) 100 nm TiO_2 nanotubes implants. (For interpretation of the references to color in this figure legend, the reader is referred to the web version of this article.)

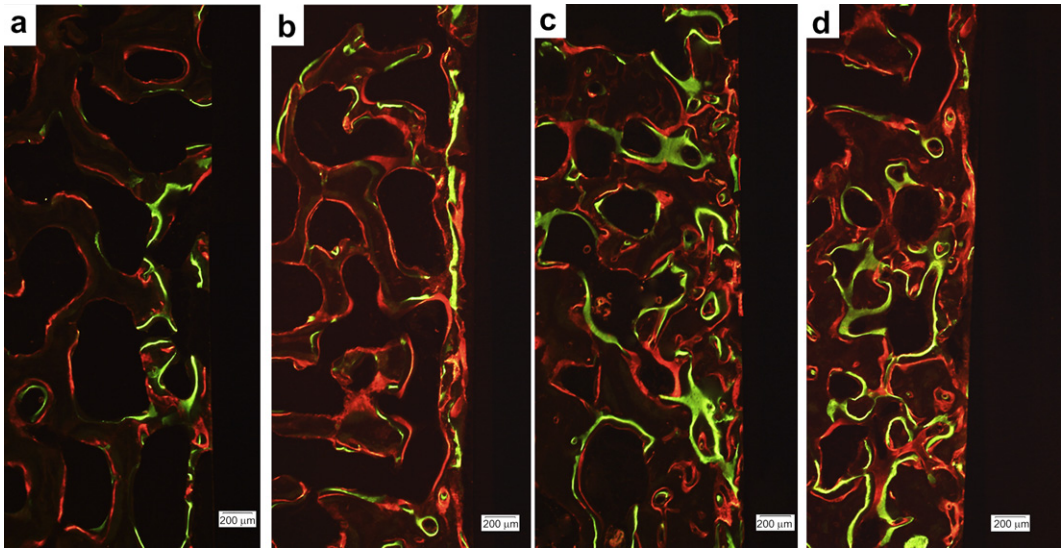

Fig. 14. Fluorescence microphotograph at 8 weeks. Fluorochrome analysis revealed new bone formation around all implants by the following markers: xylene orange-labeled lines (orange), calcein-labeled lines (green), alizarin-labeled lines (red). alizarin-labeled lines were most obvious due to the latest injection, and the xylenol orange-label was hardly detected as a result of bone metabolism. (a) Machined implant, (b) 30 nm TiO_2 nanotubes implants, (c) 70 nm TiO_2 nanotubes implants, (d) 100 nm TiO_2 nanotubes implants. (For interpretation of the references to color in this figure legend, the reader is referred to the web version of this article.)

the nature bone nanostructure, the 70 nm TiO_2 nanotubes therefore induced more osteogenesis gene expression.

In our study, the role of the distance of cells to implant was examined by comparing the gene expression of cells at the immediate vicinity of the implant surface to that detected in the peri-implant bone. At 1, 2 and 3 weeks, the effect of distance on gene expression had no significant difference, a similar pattern of gene expression between the cells of implant surface and peri-implant bone, that is, the effect of distance on gene expression was not obvious, 70 nm TiO_2 nanotubes induced more osteogenesis gene expression throughout the early stage. Nevertheless at 4 and 5 weeks after implantation, with the increase of distance of cells to implant, the role of surface regulation in gene expression weakened slightly, although the gene expression in peri-implant bone around 70 nm nanotubes was significant higher than those around 30 nm nanotubes and machined implants, the difference of gene expression between 70 nm and 100 nm nanotubes in peri-implant bone was not significant.

In the present study, the histological observations of the bone–implant interface (see Figs. 8–10) support the gene expression data, e.g. a higher degree of new bone formation is associated with TiO_2 nanotubes implants as compared to the machined ones, with the most osteogenesis occurring in interface between 70 nm nanotubes implants and bone. Based on histomorphometry analysis, the TiO_2 nanotubes surface increased the bone–implant contact and peri-implant new bone formation at 3, 5 and 8 weeks after implantation. Similar results had previously been demonstrated by other experiments [17,18]. Distance and contact osteogenesis were two phenomena of bone healing of implant [43], these two phenomena could be observed in our study (Figs. 8–10). Contact osteogenesis relies upon osteoconduction, or the recruitment and migration of differentiating osteogenic cells to the implant surface, together with *de novo* bone formation by those cells on the implant surface or down into pores or pipes [30,44]. In our study, owing to be similar to nature bone nanostructure, 70 nm nanotubes surface had superior osteoconductive ability and led to active contact osteogenesis, so the highest amount of BIC was observed with 70 nm nanotubes implants at 3, 5 and 8 weeks. The experimental data (BIC) of this study was partly different from the results in other studies [17,18], which was most likely attributed to the fact that other studies used the different animal models, the different types of implants and testing methods.

Fluorescent microscopy of the sequential fluorochrome labels revealed the dynamics of bone formation in different periods of implantation [27,45]. At 3 and 5 weeks after implantation the two fluorescent labels (xylenol orange, calcein) and calcein-labeled lines adjoining the marrow cavity were observed. Calcein was injected after the injection of xylenol orange, so calcein-labeled bone was comparatively new deposition, this result indicated that osteoblastic cells mainly originated from MSCs and the processes of bone formation were intramembranous ossification in our study. At 3 weeks after implantation (in Group I), both xylenol orange-labeled and calcein-labeled lines were very marked. At 5 weeks after implantation (in Group II), the brightness of xylenol orange-labeled lines was diminished because xylenol orange had metabolized for a longer period (21 days) than Group I, on the other hand, calcein was just injected 1 week ago, so calcein-labeled lines were more obvious than xylenol orange in Group II. At 8 weeks after implantation (in Group III), alizarin-labeled lines were most obvious due to the latest injection, and the xylenol orange-label was hardly detected as a result of bone metabolism. The sequential fluorochrome labels show that bone formation and remodeling surrounding implants occur continuously. At 3, 5 and 8 weeks, bone fluorochrome labels around TiO_2 nanotubes implants were more obvious and continuous than those around machined implants, and the fluorescent image demonstrated that new bone deposition around TiO_2 nanotubes (especially 70 nm nanotubes) implants was more rapid than that around machined ones.

5. Conclusions

TiO_2 nanotubes implants demonstrated a significant increase in new bone formation and gene expression associated with bone formation and remodeling during the osseointegration period. The differences in osteogenesis response among 30 nm, 70 nm and 100 nm nanotubes during the whole test period suggest that 70 nm

nanotube is the optimum size for TiO_2 nanotubes implants to obtain favorable osteoconductivity and osseointegration. Furthermore, TiO_2 nanotubes can control cell fate and interfacial osteogenesis by altering their nanoscale dimension, which have no dependency and side effects. At the early stage of osteogenesis, the distance from implant to cell does not influence cell regulation ability of implant surface in interfacial osteogenesis. In the experimental *in vivo* model, the combination of real-time PCR, fluorochrome labels and histological analysis provides a possibility to explore the mechanisms of osseointegration in detail. On the whole, the findings of this study explain the improved osseointegrating properties of TiO_2 nanotubes implants to a certain extent.

Acknowledgements

This work is financially supported by Natural Science Foundation of China (51002004), and City Board of Education Technology Innovation Platform (PXM2011_014226_07_000065), Beijing Municipal Commission of Education Foundation (KZ2010100050001, KM201110005003), Guangxi Natural Science Foundation (2010GXNSFB013009), and State Key Laboratory of Electronic Thin Films and Integrated Devices (UESTC: KFJJ201001).

References

[1] Mendonça G, Mendonça DB, Aragão FJ, Cooper LF. Advancing dental implant surface technology – from micron- to nanotopography. Biomaterials 2008;29:3822–35.
[2] de Jonge LT, Leeuwenburgh SC, Wolke JG, Jansen JA. Organic–inorganic surface modifications for titanium implant surfaces. Pharm Res 2008;25:2357–69.
[3] Kim HW, Koh YH, Li LH, Lee S, Kim HE. Hydroxyapatite coating on titanium substrate with titania buffer layer processed by sol–gel method. Biomaterials 2004;25:2533–8.
[4] Tamilselvi S, Raghavendran HB, Srinivasan P, Rajendran N. *In vitro* and *in vivo* studies of alkali- and heat-treated Ti–6Al–7Nb and Ti–5Al–2Nb–1Ta alloys for orthopedic implants. J Biomed Mater Res A 2009;90:380–6.
[5] Guo J, Padilla RJ, Ambrose W, De Kok IJ, Cooper LF. The effect of hydrofluoric acid treatment of TiO_2 grit blasted titanium implants on adherent osteoblast gene expression *in vitro* and *in vivo*. Biomaterials 2007;28:5418–25.
[6] Gong D, Grimes CA, Varghese OK, Hu WC, Singh RS, Chen Z, et al. Titanium oxide nanotube arrays prepared by anodic oxidation. J Mater Res 2001;16:3331–4.
[7] Mello A, Hong Z, Rossi AM, Luan L, Farina M, Querido W, et al. Osteoblast proliferation on hydroxyapatite thin coatings produced by right angle magnetron sputtering. Biomed Mater 2007;2:67–77.
[8] Daugaard H, Elmengaard B, Bechtold JE, Jensen T, Soballe K. The effect on bone growth enhancement of implant coatings with hydroxyapatite and collagen deposited electrochemically and by plasma spray. J Biomed Mater Res A 2010;92:913–21.
[9] Nayaba SN, Jonesa FH, Olsena I. Modulation of the human bone cell cycle by calcium ion-implantation of titanium. Biomaterials 2007;28:38–44.
[10] Guo YP, Zhou Y. Nacre coatings deposited by electrophoresis on Ti6Al4V substrates. Surf Coat Tech 2007;201:7505–12.
[11] Tian YS, Chen CZ, Li ST, Huo QH. Research progress on laser surface modification of titanium alloys. Appl Surf Sci 2005;242:177–84.
[12] Clair S, Variola F, Kondratenko M, Jedrzejowsk P, Nanci A, Rosei F, et al. Self-assembled monolayer of alkanephosphoric acid on nanotextured Ti. J Chem Phys 2008;128:144705–11.
[13] Mendonça G, Mendonça DB, Simões LG, Araújo AL, Leite ER, Duarte WR, et al. The effects of implant surface nanoscale features on osteoblast specific gene expression. Biomaterials 2009;30:4053–62.
[14] Biggs MJ, Richards RG, Gadegaard N, McMurray RJ, Affrossman S, Wilkinson CD, et al. Interactions with nanoscale topography: adhesion quantification and signal transduction in cells of osteogenic and multipotent lineage. J Biomed Mater Res A 2009;91:195–208.
[15] Shekaran A, Garcia AJ. Nanoscale engineering of extracellular matrix-mimetic bioadhesive surfaces and implants for tissue engineering. Biochim Biophys Acta 2011;1810:350–60.
[16] Yu W, Jiang X, Zhang F, Xu L. The effect of anatase TiO_2 nanotube layers on MC3T3-E1 preosteoblast adhesion, proliferation, and differentiation. J Biomed Mater Res A 2010;94:1012–22.
[17] Bjursten LM, Rasmusson L, Oh S, Smith GC, Brammer KS, Jin S. Titanium dioxide nanotubes enhance bone bonding *in vivo*. J Biomed Mater Res A 2010;92:1218–24.
[18] von Wilmowsky C, Bauer S, Lutz R, Meisel M, Neukam FW, Toyoshima T, et al. *In vivo* evaluation of anodic TiO2 nanotubes: an experimental study in the pig. J Biomed Mater Res B: Appl Biomater 2009;89:165–71.
[19] Oh S, Brammer KS, Li YS, Teng D, Engler AJ, Chien S, et al. Stem cell fate dictated solely by altered nanotube dimension. Proc Natl Acad Sci 2009;106:2130–5.
[20] Park J, Bauer S, Schlegel KA, Neukam FW, von der Mark K, Patrik Schmuki P. TiO_2 nanotube surfaces: 15 nm – an optimal length scale of surface topography for cell adhesion and differentiation. Small 2009;5:666–71.
[21] Brammer KS, Seunghan Oh Cobb CJ, Bjursten LM, van der Heyde H, Jin S. Improved bone-forming functionality on diameter-controlled TiO_2 nanotube surface. Acta Biomater 2009;5:3215–23.
[22] Park JW, Kim HK, Kim YJ, Jang JH, Song H, Hanawa T. Osteoblast response and osseointegration of a Ti–6Al–4V alloy implant incorporating strontium. Acta Biomater 2010;6:2843–51.
[23] Taxt-Lamolle SF, Rubert M, Haugen HJ, Lyngstadaas SP, Ellingsen JE, Monjo M. Controlled electro-implementation of fluoride in titanium implant surfaces enhances cortical bone formation and mineralization. Acta Biomater 2010;6:1025–32.
[24] Omar O, Suska F, Lennerås M, Zoric N, Svensson S, Hall J, et al. The influence of bone type on the gene expression in normal bone and at the bone-implant interface: experiments in animal model. Clin Implant Dent Relat Res; 2009:1–11.
[25] Li HY, Wang JS, Huang KL, Sun GS, Zhou ML. *In situ* preparation of multi-layer TiO_2 nanotube array thin films by anodic oxidation method. Mater Lett 2011;65:1188–90.
[26] Laiblin C, Jaeschke G. Clinical chemistry examinations of bone and muscle metabolism under stress in the Gottingen miniature pig – an experimental study. Berl Munch Tierarztl Wochenschr 1979;92:124–8.
[27] Kajiwara H, Yamaza T, Yoshinari M, Goto T, Iyama S, Atsuta I, et al. The bisphosphonate pamidronate on the surface of titanium stimulates bone formation around tibial implants in rats. Biomaterials 2005;26:581–7.
[28] McConnell D. The crystal structure of bone. Clin Orthop Relat Res 1962;23:253–68.
[29] Uchida M, Kim HM, Kokubo T, Fujibayashi S, Nakamura T. Structural dependence of apatite formation on titania gels in a simulated body fluid. J Biomed Mater Res A 2003;64:164–70.
[30] Albrektsson T, Johansson C. Osteoinduction, osteoconduction and osseointegration. Eur Spine J 2001;10:S96–101.
[31] Olivares-Navarrete R, Hyzy SL, Hutton DL, Erdman CP, Wieland M, Boyan BD, et al. Direct and indirect effects of microstructured titanium substrates on the induction of mesenchymal stem cell differentiation towards the osteoblast lineage. Biomaterials 2010;31:2728–35.
[32] Valenti MT, Carbonare LD, Donatelli L, Bertoldo F, Zanatta M, Lo Cascio V. Gene expression analysis in osteoblastic differentiation from peripheral blood mesenchymal stem cells. Bone 2008;43:1084–92.
[33] Franceschi RT, Ge C, Xiao G, Roca H, Jiang D. Transcriptional regulation of osteoblasts. Cells Tissues Organs 2007;189:196–207.
[34] Nakashima K, Zhou X, Kunkel G, Zhang Z, Deng JM, Behringer RR, et al. The novel zinc finger-containing transcription factor osterix is required for osteoblast differentiation and bone formation. Cell 2002;108:17–29.
[35] Zhang C. Transcriptional regulation of bone formation by the osteoblast-specific transcription factor Osx. J Orthop Surg Res 2010;5:37–43.
[36] Landis WJ, Hodgens KJ, Arena J, Song MJ, McEwen BF. Structural relations between collagen and mineral in bone as determined by high voltage electron microscopic tomography. Microsc Res Technol 1996;33:192–202.
[37] Minkin C. Bone acid phosphatase: tartrate-resistant acid phosphatase as a marker of osteoclast function. Calcif Tissue Int 1982;34:285–90.
[38] Hayman AR, Jones SJ, Boyde A, Foster D, Colledge WH, Carlton MB, et al. Mice lacking tartrate-resistant acid phosphatase (Acp 5) have disrupted endochondral ossification and mild osteopetrosis. Development 1996;122:3151–62.
[39] Omar OM, Lennerås ME, Suska F, Emanuelsson L, Hall JM, Palmquist A, et al. The correlation between gene expression of proinflammatory markers and bone formation during osseointegration with titanium implants. Biomaterials 2011;32:374–86.
[40] Engler AJ, Sen S, Sweeney HL, Discher DE. Matrix elasticity directs stem cell lineage specification. Cell 2006;126:677–89.
[41] Pek YS, Wan AC, Ying JY. The effect of matrix stiffness on mesenchymal stem cell differentiation in a 3D thixotropic gel. Biomaterials 2010;31:385–91.
[42] Holmes DF. Mass mapping of extracellular matrix assemblies. Biochem Soc Trans 1995;23:720–5.
[43] Osborn JF, Newesely H. Dynamic aspects of the implant–bone interface. In: Heimke G, editor. Dental implants: materials and systems. Munchen: Carl Hanser Verlag; 1980. p. 111–23.
[44] Davies JE. Understanding peri-implant endosseous healing. J Dent Educ 2003;67:932–49.
[45] Huang Y, Jin XG, Zhang XL, Sun HL, Tu JW, Tang TT, et al. *In vitro* and *in vivo* evaluation of akermanite bioceramics for bone regeneration. Biomaterials 2009;30:5041–8.